Journal of Korean Society of
Coastal and Ocean Engineers
Vol. 9, No. 4, pp. 182~193, December 1997

Interactions of a Horizontal Flexible Membrane with Incident Waves
입사파와 수평형 유연막의 상호작용

Il-Hyoung Cho*, Seok-Won Hong* and Moo Hyun Kim**
조일형* · 홍석원* · 김무현**

Abstract □ The interaction of monochromatic incident waves with a horizontal flexible membrane is investigated in the context of two-dimensional linear hydro-elastic theory. First, analytic diffraction and radiation solutions for a submerged impermeable horizontal membrane are obtained. Second, the theoretical prediction was compared with a series of experiments conducted in a two-dimensional wave tank at Texas A & M University. The measured reflection and transmission coefficients reasonably follow the trend of predicted values. Using the developed computer program, the performance of surface-mounted or submerged horizontal membrane wave barriers is tested with various system parameters and wave characteristics. It is found that the properly designed horizontal flexible membrane can be an effective wave barrier.

Keywords : breakwater, flexible membrane, reflection coefficient, transmission coefficient, model test, eigen-function expansion method, linear potential theory, diffraction, radiation

要　旨 : 본 연구에서는 유연성이 있는 막구조 방파제가 파도중 수평으로 놓여 있을 때 유연막에 의한 파랑제어 효과를 살펴보았다. 파도와 유연막의 상호작용을 고려하기 위하여 선형 유탄성 이론을 사용하였다. 계산예로 유연막의 형태, 잠긴깊이 그리고 유연막에 걸리는 초기 장력을 변화시키면서 반사율과 투과율 그리고 유연막의 변형을 살펴보았다. 또한 Texas A & M 대학의 2차원 수조에서 모형실험을 수행하여 해석해와 수치해를 비교하였다. 실험결과는 계산결과를 정성적으로 잘 따라가고 있음을 확인하였다. 개발된 설계 프로그램을 이용하여 설치 해역의 파랑 특성에 적합한 최적의 유연막 방파제를 설계.제작할 수 있으리라 사료된다.

핵심용어 : 방파제, 유연막, 반사율, 투과율, 모형실험, 고유함수전개법, 선형포텐셜 이론, 회절, 방사

1. INTRODUCTION

Most floating wave barriers are known to be ineffective in long waves unless its size is comparable to the pertinent wave length. Therefore, to be a very effective wave barrier, the structural dimension has to be large and the resulting high construction cost has been a major obstruction for the realization of many floating-breakwater projects. During the past decade, there has been a gradual increase of interest in the use of flexible plate or membrane as an effective, inexpensive wave barrier. In particular, the membrane is light and rapidly deployable, and thus it may be an ideal candidate as a portable temporary breakwater.

There have been many theoretical and experimental studies with regard to the performance of vertical flexible wave barriers. For example, the efficiency of a vertical-elastic-plate breakwater clamped at the seafloor was investigated by Lee and Chen (1990) and Williams *et al.* (1991). Abul Azm (1994) also showed that the

*한국기계연구원 선박해양공학연구센터 해양기술연구부 (Ocean Engineering Department, Korea Research Institute of Ships and Ocean Engineering, 171 Jang-dong, Yousung-ku, Taejon 305-600, Korea)
**텍사스 A & M 대학교 토목공학과 (Department of Civil Engineering, Texas A & M University, College Station, Texas 77843, USA)

efficiency of the elastic beam breakwater can be improved by tuning two vertical screens. On the other hand, the performance of a vertical-screen membrane breakwater, which is equivalent to the tensioned elastic-beam breakwater with zero bending rigidity, was investigated by Thomson *et al.* (1992), Aoki *et al.* (1994), Cho and Hong (1995), Kim and Kee (1996), Kee and Kim (1997), and Williams (1996). Using the linear wave theory and membrane-motion equation, Kim and Kee (1996) and Kee and Kim (1997) showed that almost complete reflection was possible by a vertically flexible membrane despite appreciable sinusoidal motions, which tend to generate only exponentially decaying local (evanescent) waves in the lee side. The theory was compared favorably with 2-D tank experiments (Kim *et al.*, 1996). This interesting phenomenon can also be confirmed by the classical wave-maker theory (Dean and Dalrymple, 1984).

One of the major problems associated with the use of flexible vertical screen is the expected large wave loading and possible blockage of currents. In view of this, the possibility of using alternative horizontal membrane is investigated in this paper. In particular, the submerged horizontal membrane dose not hamper the seascape and also allows the passage of ships and currents. Since the horizontal membrane does not directly block incoming waves, the diffracted and radiated waves including various elastic modes have to be properly tuned to be an effective wave barrier. The formulation of the interaction of a submerged horizontal membrane with waves is in general more complicated than the vertical-membrane case. Siew and Hurley (1977) and McIver (1985), for instance, studied the diffraction of linear waves by a submerged rigid flat plate. They showed that it can reflect significant amount of incident wave energy in a certain wave-frequency region. In this paper, it is shown that the overall wave-blocking efficiency can be greatly improved by using horizontal flexible membrane instead of rigid plate. The relevant hydro-elastic theory is formulated in Sec.2.

The present hydroelastic theory was also verified by a series of experiments conducted in a two-dimensional wave tank at Texas A & M University, which is summarized in Sec.3 It is seen that the wave-blocking performance can be reasonably predicted by the present linear hydro-elastic theory.

Finally, in Sec.4 the performance of various designs of horizontal-membrane wave barriers is studied for a variety of wave conditions or water depths. It is shown that the system can be highly efficient if properly designed and the high-performance region can be controlled by changing relevant design parameters. The results are summarized and concluding remarks are given in Sec.5

2. MATHEMATICAL FORMULATION AND ANALYTIC SOLUTIONS

We consider the interaction of a horizontal membrane wave barrier with monochromatic incident waves. Cartesian axes are chosen with the x-axis along the mean free surface and y-axis pointing vertically upwards. The water depth is denoted by h and the submergence depth of the membrane by d. It is assumed that both ends of the membrane are fixed at $x=\pm a$, and a uniform tension T is applied on the membrane in the x direction (see Fig. 1a). It is also assumed that the fluid is incompressible and inviscid, and the wave and membrane motions are small so that linear potential theory can be used. The fluid particle velocity can then be described by the gradient of a velocity potential $\Phi(x, y, t)$. Assuming harmonic motion of frequency ω, the velocity potential can be written as $\Phi(x, y, t)=Re[\phi(x, y)e^{-i\omega t}]$. Similarly, the vertical displacement of membrane can be written as

$$\zeta(x, t) = Re[(\xi(x)e^{-i\omega t}] \tag{1}$$

where $\xi(x)$ is the complex displacement of membrane.

The velocity potential ϕ satisfies the two-dimensional Laplace equation

$$\frac{\partial^2\phi}{\partial x^2} + \frac{\partial^2\phi}{\partial y^2} = 0 \quad \textit{in the fluid} \tag{2}$$

with the following boundary conditions

$$\frac{\partial \phi}{\partial y} - \nu \phi = 0 \; on \; y = 0 \;\; (\nu = \frac{\omega^2}{g}) \tag{3}$$

$$\frac{\partial \phi}{\partial y} = 0 \; on \; y = -h \tag{4}$$

$$\lim_{|x| \to \infty} (\frac{\partial \phi}{\partial x} \pm ik_1 \phi) = 0 \tag{5}$$

$$\frac{\partial \phi}{\partial y} = -i\omega\xi \; on \; y = -d, -a \le x \le a \tag{6}$$

The complex displacement of membrane can be expanded in terms of a set of natural modes of the membrane:

$$\xi(x) = \sum_{l=1}^{\infty} \varsigma_l f_l(x) \tag{7}$$

where ς_l is the unknown complex modal amplitude corresponding to the lth mode. The modal functions and eigenvalues of the membrane satisfying the membrane equation and the end condition are given by

$$f_l(x) = \begin{cases} f_l^S(x) = \cos\dfrac{\lambda_l^S x}{a}, \; \lambda_l^S = \dfrac{[2(l-1)+1]\pi}{2} \; (l = 1, 2, 3, ...) \\ f_l^A(x) = \sin\dfrac{\lambda_l^A x}{a}, \; \lambda_l^A = l\pi (l = 1, 2, 3, \cdots) \end{cases} \tag{8}$$

where the superscripts S and A denote symmetric and asymmetric modes about x=0, respectively. The modal functions given in equation (8) are orthogonal to each other in the interval [-a, a]:

$$\int_{-a}^{a} f_i(x) f_j(x) \, dx = \begin{cases} a & i = j \\ 0 & i \ne j \end{cases} \tag{9}$$

Including all the flexible membrane modes, the complex potential $\phi(x, y)$ can be expressed in the form

$$\begin{aligned} \phi(x, y) &= \phi_D(x, y) + \sum_{l=1}^{\infty} \varsigma_l \, \phi_{lR}(x, y) \\ \phi_D(x, y) &= \phi_I(x, y) + \phi_S(x, y) \end{aligned} \tag{10}$$

where ϕ_D is the diffraction potential and ϕ_S, ϕ_{lR} denote the scattering and radiation potential, respectively. The incident wave potential ϕ_I with unit amplitude is given by

$$\phi_I(x, y) = -\frac{ig}{\omega} \frac{\cosh k_1 (y + h)}{\cosh k_1 h} e^{ik_1 x} \tag{11}$$

where g is the gravitational acceleration, and k_1 is the wave number satisfying the usual dispersion relation

$$\frac{\omega^2}{g} = k_1 \tanh k_1 h \tag{12}$$

2.1 Diffraction Problem

The diffraction potential ϕ_D satisfies equation (2)-(5) and the following membrane boundary condition:

$$\frac{\partial \phi_D}{\partial y} = 0 \;\; on \;\; y = -d, -a \le x \le a \tag{13}$$

In the following, the symmetry of the fluid and membrane is used by splitting ϕ_D into symmetric and asymmetric parts.

$$\phi_D(x, y) = \phi_D^S(x, y) + \phi_D^A(x, y) \tag{14}$$

where

$$\phi_D^S(-x, y) = \phi_D^S(x, y), \; \frac{\partial \phi_D^S}{\partial x} = 0 \;\; on \;\; x = 0$$

$$\phi_D^A(-x, y) = -\phi_D^A(x, y), \; \phi_D^A = 0 \;\; on \;\; x = 0$$

The fluid domain is divided into three regions, as shown in Fig. 1a. Region (I) is defined by $x \le -a$, $-h < y < 0$, region (II) by $|x| \le a$, $-d < y < 0$ and region (III) by $|x| \le a$, $-h < y < -d$.

The symmetric diffraction potentials in the three fluid regions are written as

$$\begin{aligned} \phi_D^{S(1)} &= -\frac{ig}{\omega} \{\frac{1}{2} e^{-k_{10}x} f_{10}(y) + \sum_{n=0}^{\infty} a_n^S e^{k_{1n}(x+a)} f_{1n}(y)\} \\ \phi_D^{S(2)} &= -\frac{ig}{\omega} \sum_{n=0}^{\infty} b_n^S \cosh k_{2n} x \, f_{2n}(y) \\ \phi_D^{S(3)} &= -\frac{ig}{\omega} \{c_0^S f_{30}(y) + \sum_{n=1}^{\infty} c_n^S \cosh k_{3n} c \, f_{3n}(y)\} \end{aligned} \tag{15}$$

where $k_{10} = -ik_1$, $k_{20} = -ik_2$

The eigenfunctions $f_{1n}(y)$, $f_{2n}(y)$, and $f_{3n}(y)$ are given by

$$f_{1n}(y) = \begin{cases} \dfrac{\cosh k_1 (y + h)}{\cosh k_1 h}, & n = 0 \\ \dfrac{\cos k_{1n} (y + h)}{\cos k_{1n} h}, & n \ge 1 \end{cases} \tag{16}$$

$$f_{2n}(y)=\begin{cases}\dfrac{\cosh k_2(y+d)}{\cosh k_2 d}, & n=0\\ \dfrac{\cos k_{2n}(y+d)}{\cos k_{2n} d}, & n\geq 1\end{cases} \tag{17}$$

$$f_{3n}(y)=\frac{\cos k_{3n}(y+h)}{\cos k_{3n}(h-d)} \qquad n\geq 0 \tag{18}$$

The eigenvalues k_{1n}, k_{2n}, k_{3n} are the solutions of the following equations

$$\begin{cases} k_1 \tanh k_1 h = \dfrac{\omega^2}{g}, & n=0\\ k_{1n}\tan k_{1n} h = -\dfrac{\omega^2}{g}, & n\geq 1\end{cases} \tag{19}$$

$$\begin{cases} k_2 \tanh k_2 d = \dfrac{\omega^2}{g}, & n=0\\ k_{2n}\tan k_{2n} d = -\dfrac{\omega^2}{g}, & n\geq 1\end{cases} \tag{20}$$

$$k_{3n}=\frac{n\pi}{(h-d)},\ n\geq 0 \tag{21}$$

The unknown coefficients a_n^S, b_n^S, $c_n^S (n=0, 1, 2, \cdots)$ can then be determined by invoking the continuity of potential and horizontal velocity at $x=-a$. The continuity of ϕ_D^S at $x=-a$ requires that

$$\frac{1}{2}e^{k_{10}a} f_{10}(y)+\sum_{n=0}^{\infty} a_n^S f_{1n}(y)= \tag{22a, b}$$
$$\begin{cases}\displaystyle\sum_{n=0}^{\infty} b_n^S \cosh k_{2n} a\ f_{2n}(y), & -d\leq y\leq 0\\ c_0^S f_{30}(y)+\displaystyle\sum_{n=1}^{\infty} c_n^S \cosh k_{3n} a\ f_{3n}(y), & -h\leq y\leq -d\end{cases}$$

Multiplying (22a) $f_{2m}(y)$ by and integrating with respect to y over [-d, 0], we obtain

$$b_m^S \cosh k_{2m} a\ N_m^{(2)}=\frac{1}{2}e^{k_{10}a} C_{m0}+\sum_{n=0}^{\infty} a_n^S C_{mn} \tag{23a}$$

where

$$C_{mn}=\int_{-d}^{0} f_{1n}(y) f_{2m}(y)dy$$
$$\int_{-d}^{0} f_{2n}(y) f_{2m}(y)dy=\begin{cases}N_m^{(2)}, & m=n\\ 0, & m\neq n\end{cases} \tag{23b}$$

If we multiply (22b) by $f_{3m}(y)$ and integrate with respect to y from -h to -d, the following equation can be obtained.

$$m=0:\ c_0^S N_0^{(3)}=\frac{1}{2}e^{k_{10}a} D_{00}+\sum_{n=0}^{\infty} a_n^S D_{0n}$$
$$m\neq 0:\ c_m^S \cosh k_{3m} a\ N_m^{(3)}=\frac{1}{2}e^{k_{10}a} D_{m0}+\sum_{n=0}^{\infty} a_n^S D_{mn} \tag{24a}$$

where

$$D_{mn}=\int_{-h}^{-d} f_{1n}(y) f_{3m}(y)dy$$
$$\int_{-h}^{-d} f_{3n}(y) f_{3m}(y)dy=\begin{cases}N_m^{(3)}, & m=n\\ 0, & m\neq n\end{cases} \tag{24b}$$

On the other hand, the continuity of $\partial\phi_D^S/\partial x$ at $x=-a$ gives

$$-\frac{1}{2}k_{10}e^{k_{10}a} f_{10}(y)+\sum_{n=0}^{\infty} k_{1n} a_n^S f_{1n}(y)=$$
$$\begin{cases}\displaystyle -\sum_{n=0}^{\infty} k_{2n} b_n^S \sinh k_{2n} a\ f_{2n}(y), & -d\leq y\leq 0\\ \displaystyle -\sum_{n=0}^{\infty} k_{3n} c_n^S \sinh k_{3n} a\ f_{3n}(y), & -h\leq y\leq -d\end{cases} \tag{25}$$

Multiplying both sides of equation (25) by $f_{1m}(y)$ and integrating with respect to y from -h to 0, we obtain

$$m=0:$$
$$-\frac{1}{2}k_{10}e^{k_{10}a} N_0^{(1)}+k_{10} a_0^S N_0^{(1)}=-\sum_{n=0}^{\infty} k_{2n} b_n^S \sinh k_{2n} a C_{n0}$$
$$-\sum_{n=1}^{\infty} k_{3n} c_n^S \sinh k_{3n}\ a D_{n0} \tag{26}$$
$$m\neq 0:$$
$$k_{1m} a_m^S N_m^{(1)}=-\sum_{n=0}^{\infty} k_{2n}\ b_n^S \sinh k_{2n} a\ C_{nm}$$
$$-\sum_{n=1}^{\infty} k_{3n} c_n^S \sinh k_{3n} a D_{nm}$$

where

$$\int_{-h}^{0} f_{1n}(y) f_{1m}(y)dy=\begin{cases}N_m^{(1)}, & m=n\\ 0, & m\neq n\end{cases}$$

The final matrix equation for a_k^S can then be obtained by substituting equations (23) and (24) into equation (26):

$$a_0^S+\sum_{k=0}^{\infty}\frac{F_{ok}^S}{k_{10}N_0^{(1)}}a_k^S=-\frac{1}{2}e^{k_{10}a}\left(\frac{F_{00}^S}{k_{10}N_0^{(1)}}-1\right),\quad m=0$$

$$a_m^S+\sum_{k=0}^{\infty}\frac{F_{mk}^S}{k_{1m}N_m^{(1)}}a_k^S=-\frac{1}{2}e^{k_{1m}a}\frac{F_{m0}^S}{k_{1m}N_m^{(1)}},\quad m=1,2,3,\cdots \tag{27a}$$

where

$$F_{mk}^S=\sum_{n=0}^{\infty}\frac{k_{2n}\tanh k_{2n}aC_{nm}C_{nk}}{N_n^{(2)}}+\sum_{n=1}^{\infty}\frac{k_{3n}\tanh k_{3n}aD_{nm}D_{nk}}{N_n^{(3)}} \tag{27b}$$

By solving the above simultaneous algebraic equations, the unknown constants a_n^S can be determined. Subsequently, the other unknown constants b_n^S, c_n^S can be derived from equations (22) and (23) as follows:

$$b_n^S=\frac{\left(\frac{1}{2}e^{k_{10}a}C_{n0}+\sum_{k=0}^{\infty}a_k^SC_{nk}\right)}{\cosh k_{2n}a\,N_n^{(2)}},\quad n\geq 0$$

$$c_n^S=\begin{cases}\dfrac{\left(\frac{1}{2}e^{k_{10}a}D_{00}+\sum_{k=0}^{\infty}a_k^SD_{0k}\right)}{N_0^{(3)}}, & n=0\\ \dfrac{\left(\frac{1}{2}e^{k_{10}a}D_{n0}+\sum_{k=0}^{\infty}a_k^SD_{nk}\right)}{\cosh k_{3n}aN_n^{(3)}}, & n\geq 1\end{cases} \tag{28}$$

Similarly, the asymmetric diffraction potentials in the three fluid regions are written as

$$\phi_D^{A(1)}=-\frac{ig}{\omega}\left\{\frac{1}{2}e^{-k_{10}x}f_{10}(y)+\sum_{n=0}^{\infty}a_n^Ae^{k_{1n}(x+a)}f_{1n}(y)\right\}$$

$$\phi_D^{A(2)}=-\frac{ig}{\omega}\sum_{n=0}^{\infty}b_n^A\sinh k_{2n}x\,f_{2n}(y) \tag{29}$$

$$\phi_D^{A(3)}=-\frac{ig}{\omega}\left\{c_0^A\left(\frac{x}{a}\right)f_{30}(y)+\sum_{n=1}^{\infty}c_n^A\sinh k_{3n}x\,f_{3n}(y)\right\}$$

The unknown coefficients a_n^A, b_n^A, c_n^A ($n=0, 1, 2, \cdots$) can be determined in a similar manner by applying the continuity of potentials and horizontal velocities on $x=-a$:

$$a_0^A+\sum_{k=0}^{\infty}\frac{F_{0k}^A}{k_{10}N_0^{(1)}}a_k^A=-\frac{1}{2}e^{k_{10}a}\left(\frac{F_{00}^A}{k_{10}N_0^{(1)}}-1\right),\quad m=0$$

$$a_m^A+\sum_{k=0}^{\infty}\frac{F_{mk}^A}{k_{1m}N_m^{(1)}}a_k^A=-\frac{1}{2}e^{k_{1m}a}\frac{F_{m0}^A}{k_{1m}N_m^{(1)}},\quad m=1,2,3,\cdots \tag{30a}$$

where

$$F_{mk}^A=\sum_{n=0}^{\infty}\frac{k_{2n}\coth k_{2n}aC_{nm}C_{nk}}{N_n^{(2)}}+\frac{D_{0m}D_{0k}}{aN_0^{(3)}}+\sum_{n=1}^{\infty}\frac{k_{3n}\coth k_{3n}aD_{nm}D_{nk}}{N_n^{(3)}} \tag{30b}$$

The remaining unknown coefficients b_n^A and c_n^A can then be determined from:

$$b_n^A=-\frac{\left(\frac{1}{2}e^{k_{10}a}C_{n0}+\sum_{k=0}^{\infty}a_k^AC_{mk}\right)}{\sinh k_{2n}aN_n^{(2)}},\quad n\geq 0$$

$$c_n^A=\begin{cases}-\dfrac{\left(\frac{1}{2}e^{k_{10}a}D_{00}+\sum_{k=0}^{\infty}a_k^AD_{0k}\right)}{N_0^{(3)}}, & n=0\\ -\dfrac{\left(\frac{1}{2}e^{k_{10}a}D_{n0}+\sum_{k=0}^{\infty}a_k^AD_{nk}\right)}{\sinh k_{3n}aN_n^{(3)}}, & n\geq 1\end{cases} \tag{31}$$

2.2 Radiation Problem

The radiation potential of each mode, ϕ_{IR}, is governed by (2)-(5) and the following body-boundary condition:

$$\frac{\partial\phi_{IR}}{\partial y}=-i\omega f_I(x)\ \ on\ \ y=-d\ \ -a\leq x\leq a \tag{32}$$

For simplicity, we split ϕ_{IR} into symmetric and asymmetric parts as in the diffraction problem:

$$\phi_{IR}(x,y)=\phi_{IR}^S(x,y)+\phi_{IR}^A(x,y) \tag{33}$$

The radiation potentials in regions (II) and (III) can be represented by the sum of homogeneous solution and particular solution. The homogeneous solutions look similar to those considered in the diffraction problem. The symmetric radiation potentials in each region can be written as

$$\phi_{IR}^{S(1)}=-\frac{ig}{\omega}\sum_{n=0}^{\infty}a_{In}^Se^{k_{1n}(x+a)}f_{1n}(y)$$

$$\phi_{IR}^{S(2)}=-\frac{ig}{\omega}\left\{\sum_{n=0}^{\infty}b_{In}^S\cosh k_{2n}x\,f_{2n}(y)+\frac{i\omega}{g}\tilde{\phi}_{IR}^{S(2)}(x,y)\right\}$$

$$\phi_{IR}^{S(3)}=-\frac{ig}{\omega}\left\{c_{I0}^Sf_{30}(y)+\sum_{n=1}^{\infty}c_{In}^S\cosh k_{3n}x\,f_{3n}(y)+\frac{i\omega}{g}\tilde{\phi}_{IR}^{S(3)}(x,y)\right\} \tag{34}$$

The asymmetric radiation potentials can be expressed in a similar manner:

$$\phi_{lR}^{A(1)}=-\frac{ig}{\omega}\sum_{n=0}^{\infty}a_{ln}^{A}e^{k_{ln}(x+a)}f_{1n}(y)$$

$$\phi_{lR}^{A(2)}=-\frac{ig}{\omega}\{\sum_{n=0}^{\infty}b_{ln}^{A}\sinh k_{2n}x\,f_{2n}(y)+\frac{i\omega}{g}\tilde{\phi}_{lR}^{A(2)}(x,y)\} \quad (35)$$

$$\phi_{lR}^{A(3)}=-\frac{ig}{\omega}\{c_{l0}^{A}(\frac{x}{a})f_{30}(y)+\sum_{n=1}^{\infty}c_{ln}^{A}\sinh k_{3n}xf_{3n}(y)+\frac{i\omega}{g}\tilde{\phi}_{lR}^{A(3)}(x,y)\}$$

The particular solutions in (II) and (III) satisfying the inhomogeneous body-boundary condition can be obtained as

$$\tilde{\phi}_{lR}^{S(2)}(x,y)=\frac{-i\omega\cos(\lambda_l^S x/a)[(\lambda_l^S/a)\cosh(\lambda_l^S y/a)+\nu\sinh(\lambda_l^S y/a)]}{(\lambda_l^S/a)[-(\lambda_l^S/a)\sinh(\lambda_l^S d/a)+\nu\cosh(\lambda_l^S d/a)]} \quad (36)$$

$$\tilde{\phi}_{lR}^{A(2)}(x,y)=\frac{-i\omega\sin(\lambda_l^A x/a)[(\lambda_l^A/a)\cosh(\lambda_l^A y/a)+\nu\sinh(\lambda_l^A y/a)]}{(\lambda_l^A/a)[-(\lambda_l^A/a)\sinh(\lambda_l^A d/a)+\nu\cosh(\lambda_l^A d/a)]} \quad (37)$$

$$\tilde{\phi}_{lR}^{S(3)}(x,y)=\frac{-i\omega\cos(\lambda_l^S x/a)\cosh[(\lambda_l^S/a)(y+h)]}{(\lambda_l^S/a)\sinh[(\lambda_l^S/a)(h-d)]} \quad (38)$$

$$\tilde{\phi}_{lR}^{A(3)}(x,y)=\frac{-i\omega\sin(\lambda_l^A x/a)\cosh[(\lambda_l^A/a)(y+h)]}{(\lambda_l^A/a)\sinh[(\lambda_l^A/a)(h-d)]} \quad (39)$$

The unknown constants in equations (34) and (35) can be determined in a similar manner to the diffraction problem using the matching conditions at $x=-a$. The simultaneous algebraic equations for the unknown constants $a_{lk}^{S,A}$ in region (I) are given by

$$a_{lm}^{S,A}+\sum_{k=0}^{\infty}\frac{F_{mk}^{S,A}}{k_{1m}N_m^{(1)}}a_{lk}^{S,A}=\frac{X_{ml}^{S,A}}{k_{1m}N_m^{(1)}}\quad(m=0,1,2,3,\cdots) \quad (40)$$

where

$$X_{ml}^{S,A}=\frac{i\omega}{g}\{\int_{-d}^{0}\frac{\partial\tilde{\phi}_{lR}^{S,A(2)}(-a,y)}{\partial x}f_{1m}(y)dy+\int_{-h}^{-d}\frac{\partial\tilde{\phi}_{lR}^{S,A(3)}(-a,y)}{\partial x}f_{1m}(y)dy\} \quad (41)$$

The other unknown coefficients can be determined from

$$b_{ln}^{S}=-\frac{\{\frac{i\omega}{g}\int_{-d}^{0}\tilde{\phi}_{lR}^{S(2)}f_{2n}(y)dy-\sum_{k=0}^{\infty}a_{lk}^{S}C_{nk}\}}{\cosh k_{2n}aN_n^{(2)}},\quad n\geq 0$$

$$c_{ln}^{S}=\begin{cases}-\dfrac{\{\frac{i\omega}{g}\int_{-h}^{-d}\tilde{\phi}_{lR}^{S(3)}f_{30}(y)dy-\sum_{k=0}^{\infty}a_{lk}^{S}D_{0k}\}}{N_0^{(3)}}, & n=0\\ -\dfrac{\{\frac{i\omega}{g}\int_{-h}^{-d}\tilde{\phi}_{lR}^{S(3)}f_{3n}(y)dy-\sum_{k=0}^{\infty}a_{lk}^{S}D_{nk}\}}{\cosh k_{3n}aN_n^{(3)}}, & n\geq 1\end{cases} \quad (42a)$$

and

$$b_{ln}^{A}=\frac{\{\frac{i\omega}{g}\int_{-d}^{0}\tilde{\phi}_{lR}^{A(2)}f_{2n}(y)dy-\sum_{k=0}^{\infty}a_{lk}^{A}C_{nk}\}}{\sinh k_{2n}aN_n^{(2)}},\quad n\geq 0$$

$$c_{ln}^{A}=\begin{cases}\dfrac{\{\frac{i\omega}{g}\int_{-h}^{-d}\tilde{\phi}_{lR}^{A(3)}f_{30}(y)dy-\sum_{k=0}^{\infty}a_{lk}^{A}D_{0k}\}}{N_0^{(3)}}, & n=0\\ \dfrac{\{\frac{i\omega}{g}\int_{-h}^{-d}\tilde{\phi}_{lR}^{A(3)}f_{3n}(y)dy-\sum_{k=0}^{\infty}a_{lk}^{A}D_{nk}\}}{\sinh k_{3n}aN_n^{(3)}}, & n\geq 1\end{cases} \quad (42b)$$

2.3 Membrane Response

Neglecting viscous (or material) damping, the motion of membrane is governed by the inhomogeneous one-dimensional wave equation as follows:

$$T\frac{d^2\xi}{dx^2}+m\omega^2\xi=-i\rho\omega[\phi^{(3)}(x,d)-\phi^{(2)}(x,-d)] \quad (43)$$

where T, ρ, and m are the membrane tension, fluid density, and membrane mass per unit length, respectively. Substituting $\phi(x,y)=\phi_D(x,y)+\sum_{j=1}^{\infty}\varsigma_j\phi_{jR}(x,y)$, $\xi(x)=\sum_{j=1}^{\infty}\varsigma_j f_j(x)$ into (43) yields

$$\sum_{j=1}^{\infty}\varsigma_j\{-T\frac{d^2f_j(x)}{dx^2}-m\omega^2 f_j(x)-p_{jR}(x)\}=p_D(x) \quad (44a)$$

where

$$p_{jR}(x)=i\rho\omega[\phi_{jR}^{(3)}(x,-d)-\phi_{jR}^{(2)}(x,-d)]$$
$$p_D(x)=i\rho\omega[\phi_D^{(3)}(x,-d)-\phi_D^{(2)}(x,-d)] \quad (44b)$$

Multiplying the above equation by $f_i(x)$ and integra-

ting over the membrane, we obtain

$$\sum_{j=1}^{\infty}\{K_{ij}-\omega^2(M_{ij}+\hat{a}_{ij})-i\omega\hat{b}_{ij}\}\varsigma_j=F_i,\ i=1,2,3,\cdots \tag{45a}$$

where

$$\begin{aligned}
K_{ij}&=-\int_{-a}^{a}T\frac{d^2f_j(x)}{dx^2}f_i(x)dx\\
M_{ij}&=\int_{-a}^{a}mf_j(x)f_i(x)dx\\
\hat{a}_{ij}&=\mathrm{Re}\{\frac{1}{\omega^2}\int_{-a}^{a}p_{jR}(x)f_i(x)dx\}\\
\hat{b}_{ij}&=\mathrm{Im}\{\frac{1}{\omega}\int_{-a}^{a}p_{jR}(x)f_i(x)dx\}\\
F_i&=\int_{-a}^{a}p_D(x)f_i(x)dx
\end{aligned} \tag{45b}$$

The symbols K_{ij}, M_{ij} and F_i represent the generalized (modal) stiffness matrix, mass matrix and force vector, respectively, and $\hat{a}_{ij}$ and $\hat{b}_{ij}$ are the generalized added-mass and radiation-damping matrix. Truncating the series of (45a) at the appropriate term M, we can solve for the unknown complex amplitudes ς_j corresponding to each mode. When the membrane is on the free surface, a hydrostatic correction term needs to be added.

Finally, the reflection and transmission coefficients can be determined from

$$\begin{aligned}
R_f&=|[(a_0^S+a_0^A)+\sum_{l=1}^{M}\varsigma_l(a_{lR}^S+a_{lR}^A)]e^{k_{1l}a}|\\
T_r&=|[(a_0^S+a_0^A)+\sum_{l=1}^{M}\varsigma_l(a_{lR}^S+a_{lR}^A)]e^{k_{1l}a}|
\end{aligned} \tag{46}$$

The vertical hydrodynamic forces on the horizontal membrane can be calculated from

$$F=-i\rho\omega\int_{-a}^{a}[\phi^{(3)}(x,-d)-\phi^{(2)}(x,-d)]dx \tag{47}$$

3. EXPERIMENTS

In order to validate the theory and numerical procedure developed in the preceding section, we conducted a series of experiments in the two-dimensional wave tank (37 m long, 0.91 m wide, and 1.22 m deep) located at Texas A&M University. The glass-walled wave tank is equipped with a dry-back, hinged flap wave maker capable of producing regular and irregular waves.

The wave elevation was measured with a resistance wave gauge having an accuracy of ± 0.1 cm. A probe measuring incident and reflected wave heights and another probe measuring the transmitted wave heights are placed at 9.1 m and 22.9 m from the wavemaker, respectively. The wave barrier model was placed at 18.3 m from the wavemaker between the two probes. Regular waves were generated by a user-defined time-voltage input to the wave maker. The wave frequency range used in our experiments was from 0.5 to 1.4 Hz. The wave heights used in our experiments are 6 cm, 8 cm and 10 cm, respectively. The time series of the generated regular wave packet was sinusoidal with the beginning and end of the series attenuated in amplitude.

The model membrane (m=0.17 kg/m^2) was made of a thin plastic material resembling a plastic tarpaulin. The length and width of the membrane were 80 cm and 82 cm, respectively. The ends of the membrane were attached to two horizontal steel bars which are fixed by four vertical steel frames clamped to the tank, as shown in Fig. 1b. The tension on the membrane was provided by a series of string-weight units. The end-bar

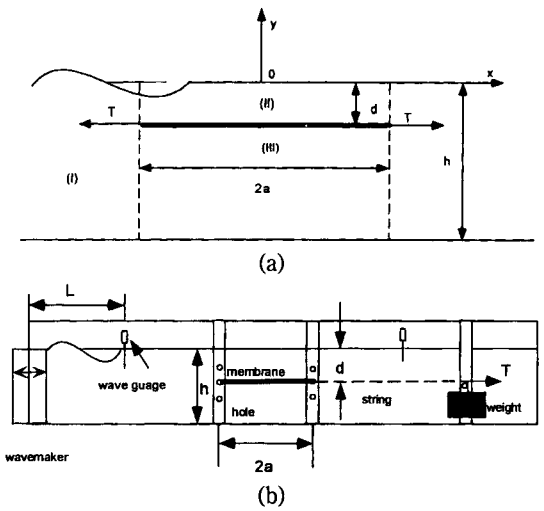

Fig. 1. (a) Definition sketch for horizontal impermeable flexible membrane, (b) Experimental set-up of a submerged horizontal membrane breakwater.

Table 1. Experimental Conditions.

	Exp. #1	Exp. #2	Exp. #3
Membr. Length (cm)	80	80	80
Membr. Width (cm)	82	82	82
Subm. Depth (cm)	16	16	0
Water Depth (cm)	80	80	56
Membr. Tension (kgF)	36	21	36
Wave Frequency (Hz)	0.5-1.4	0.5-1.4	0.5-1.4
Wave Amplitude (cm)	3, 4, 5	3	3

of the tensioned membrane was then fixed to a new location of the steel frame. After a tension is correctly given, the string-weight units were removed. Table 1 summarizes the principal characteristics of the models used in our experiments.

The signal of the incident wave train was obtained as it passes the probe toward the membrane breakwater. Then, the reflected wave train was recorded as the reflected waves pass the probe again in the opposite direction. After averaging the wave heights for the incident and reflected, and transmitted wave trains, the reflection coefficient R_f and transmission coefficient T_r can be calculated from the ratio of the averaged reflected and transmitted wave height to the averaged incident wave height. We observed that reflected and transmitted waves were repeatedly reflected from the wave maker and beach as the time goes on. In order to minimize the effects of multiple reflection, the present method was adopted in favor of moving single probe method or three-probe method (Isaacson, 1991), which require relatively longer time to establish a steady state. It is shown in Hagen (1994) that the present method is more reliable than the moving-probe or three-probe methods when nonlinear phenomena or multiple reflections exist. In most of our surface-piercing-buoy experiments, the errors estimated from the energy relation were able to be kept within 10%. The discrepancy can be attributed to viscous, gap, and nonlinear effects, and membrane material damping etc. When the membrane is located on or very close to the calm water level, the energy-conservation error is increased due to wave overtopping over the membrane.

4. NUMERICAL RESULTS AND DISCUSSIONS

The analytic solutions for impermeable membrane were developed as described in Sec. 2. First, the convergence of analytic solutions with the number of natural modes M and eigenfunctions N is shown in Fig. 2. It is seen that the convergence with those parameters is rapid. In the following, the analytic solutions with M =5, N=10 were used to investigate the performance of a horizontal flexible membrane wave barrier for various design conditions. The membrane mass per unit length used for these numerical examples was 1.0 kg/m^2.

In Fig. 3a and 3b, the transmission coefficients and hydrodynamic loading on a particular membrane are plotted for various membrane tensions. It is seen that there exists an optimal tension for the given design

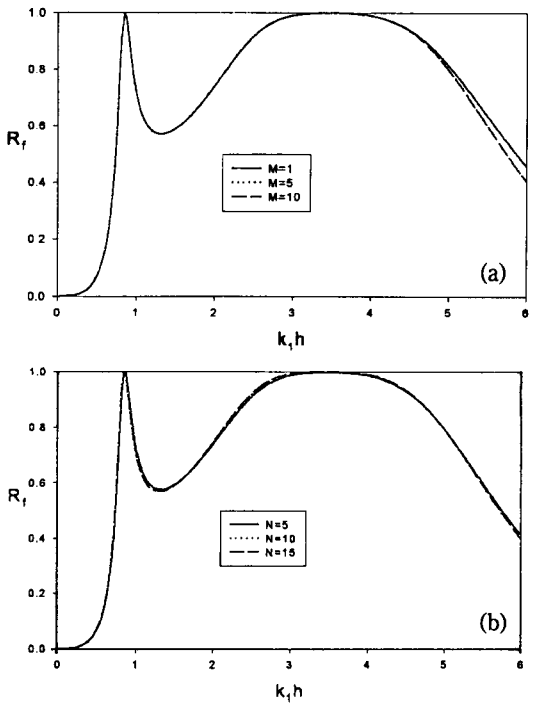

Fig. 2. (a) Convergence of reflection coefficient with the number of natural modes of membrane for the case d/h=0.2, a/h=0.5, $T/\rho gh^2$=0.1 and N=10 (N= number of eigenfunctions), (b) Convergence of reflection coefficient with the number of eigenfunctions for the case d/h=0.2, a/h=0.5, $T/\rho gh^2$=0.1 and M=5.

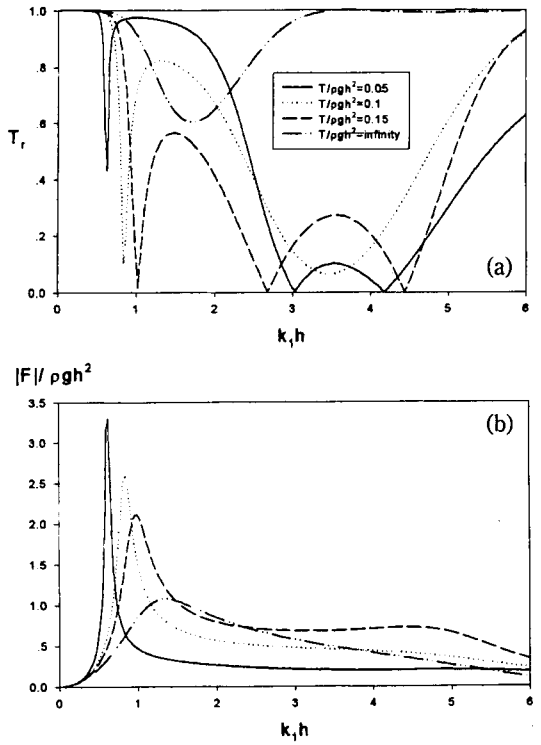

Fig. 3. Transmission coefficient (a) and hydrodynamic loading (b) of a submerged horizontal membrane breakwater as function of non-dimensional tension $T/\rho gh^2$ and wavenumber k_1h for d/h=0.2, a/h=0.5.

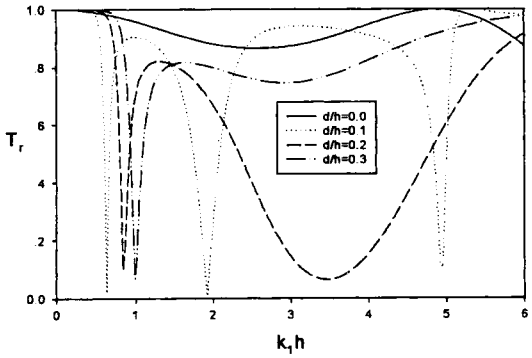

Fig. 4. Transmission coefficients of a submerged impermeable membrane breakwater as function of submergence depth d/h and wavenumber k_1h for a/h= 0.5, $T/\rho gh^2$=0.1.

condition. The infinite-tension case corresponds to the diffraction by a rigid horizontal plate which was also studied by McIver (1985) for the normal incidence case. The correctness of the limiting case was also checked against McIver's results. In Fig. 3(b), the hydrodynamic loading for the lower tension (or more flexible membrane) tends to be smaller but has a larger peak near the resonance region.

In Fig. 4, the membrane tension and width are fixed and the submergence depth is varied from 0 to 0.3 h. For this example, the overall efficiency is best for the case d=0.2 h. The trend of the limiting case d=0 (membrane on the water surface) is quite different from that of the other curves because only the lower part of the surface-mounted membrane is exposed to the fluid loading. In Fig. 5, the amplitudes of membrane responses ($|\xi|/A$) are plotted for the cases d=0.1 h and 0.2 h as function of dimensionless x coordinate and wavenumbers. It is interesting to see that the performance is still good near k_1h=1 despite large sinusoidal membrane motions. The motion amplitudes are much smaller than the incident wave amplitude except for the resonance region. The modal amplitudes for each mode are plotted in Fig. 6 for the case d=0.2 h.

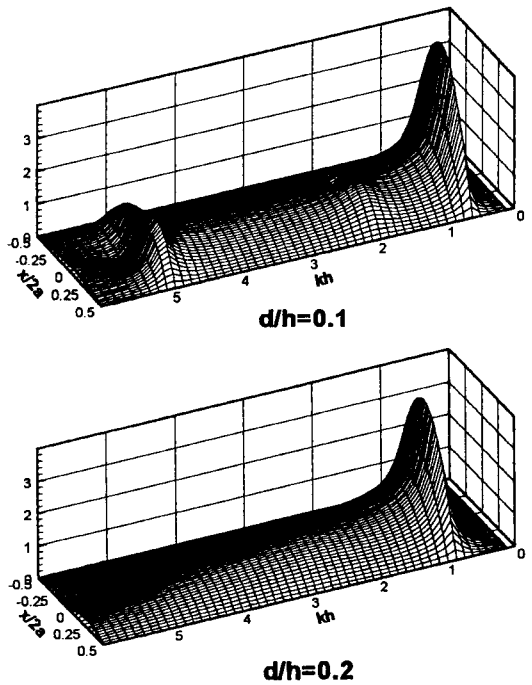

Fig. 5. Responses of a membrane ($|\xi|/A$) as function of wavenumber k_1h and horizontal coordinate $x/2a$ for d/h=0.1, and 0.2, a/h=0.5, $T/\rho gh^2$=0.1.

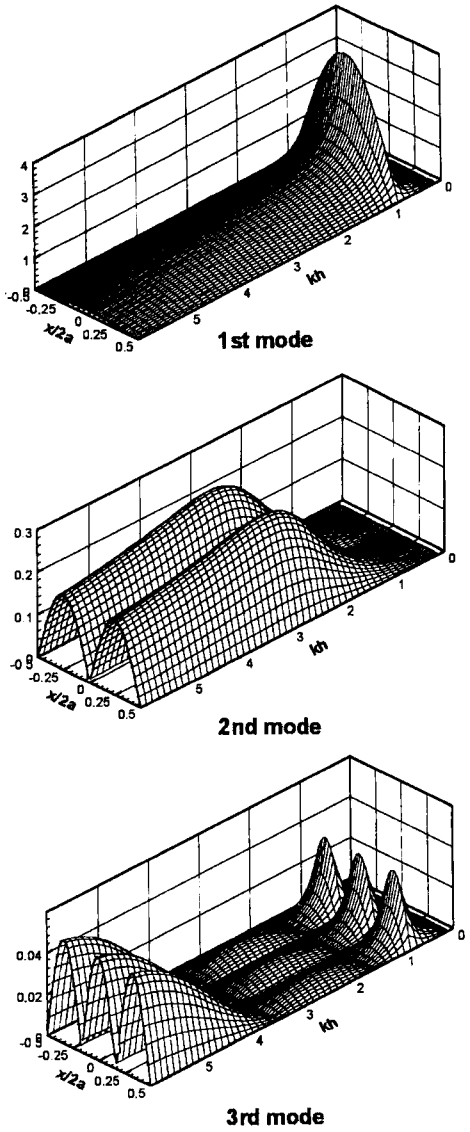

Fig. 6. Modal response amplitude as function of wavenumber k_1h and horizontal coordinate $x/2a$ for d/h= 0.2, a/h=0.5, T/ρgh^2=0.1.

It is shown that the modal amplitudes of higher harmonics are rapidly decreased.

In the next figure (Fig. 7), the membrane tension and submergence depth are fixed and the size (width) of membrane is varied from a=0.3 h to 0.6 h. Interestingly, the bandwidth of the high performance region is largest when a=0.4 h, which implies that the efficiency is not necessarily improved with the size of membrane.

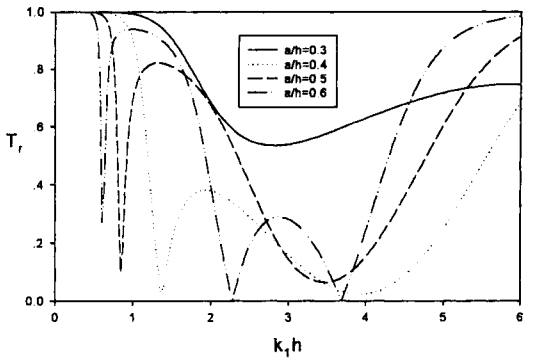

Fig. 7. Transmission coefficients of a submerged impermeable membrane breakwater as function of length of membrane a/h and wavenumber k_1h for d/h=0.2, T/ρgh^2=0.1.

However, the non-total transmission region can be extended to longer waves as the size increases.

Finally, the computational results for impermeable membrane are compared with the experimental results conducted in the 2D wave tank located at Texas A&M University. The measured values generally follow the trend of computed curves. The same experiment was conducted for three different incident wave amplitudes, and the general trend looks similar. It can be seen in Fig. 8 that the wave blocking performance is indeed good in the range $0.8 < f < 1.3$ (Hz), as predicted by the present linear hydro-elastic theory. We can notice that its effect is the largest near the resonance region ($f \approx 0.35$ Hz). The discrepancy between predicted and

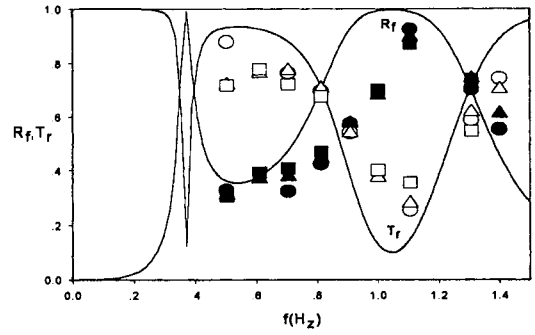

Fig. 8. Comparison of analytic results with measured values (Exp. 1) for a submerged horizontal membrane breakwater; analytic solutions (———), experimental results R_f (dark) and T_r (white) (circle: 3 cm, triangle: 4 cm, square: 5 cm).

measured results can be attributed to the uncertainties pertaining to the amount of viscous (or material) damping, nonlinear effects, gap or end effects etc. In particular, we observed during the experiment that the membrane response was not perfectly uniform in the y direction. Fig. 9 shows similar comparisons for smaller membrane tension. Again, the measured values generally follow predicted values. The wave blocking efficiency in this case is very good when $f > 0.8$ Hz and near $f \approx 0.3$ Hz. The next figure (Fig. 10) shows similar comparisons for the surface-mounted membrane. The performance of this particular design is not good unless $f > 1.2$ Hz. For this particular case, the wave overtopping over the surface-mounted membrane adds more uncertainty with regard to the validity of the present theoretical model. Despite the additional uncertainty, the trend of experimental values follows reasonably that of predicted values.

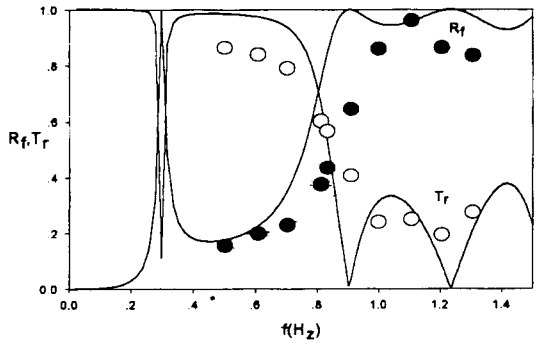

Fig. 9. Comparison of analytic results with measured values (Exp. 2) for a submerged horizontal membrane breakwater; analytic solution (——), experimental Results R_f (dark) and T_r (white).

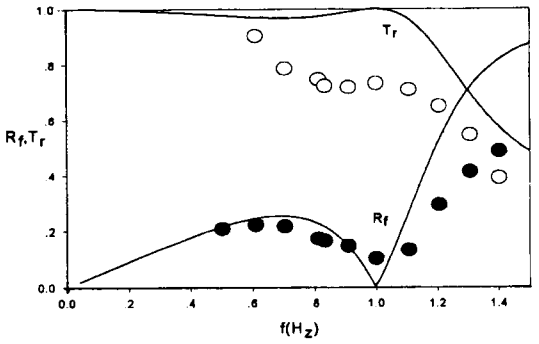

Fig. 10. Comparison of analytic results with measured values (Exp. 3) for a floating horizontal membrane breakwater; analytic solution (——), experimental results R_f (dark) and T_r (white).

5. SUMMARY AND CONCLUSIONS

The interaction of monochromatic incident waves with a horizontal flexible membrane was investigated in the context of two-dimensional linear hydro-elastic theory. In Sec.2, analytic diffraction and radiation solutions for a submerged impermeable horizontal membrane were obtained by matching the eigenfunction solutions in the three fluid domains. The linear hydro-elastic theory was then compared with a series of experiments conducted with an impermeable membrane and a reasonable agreement was obtained.

Using the developed computer program, the performance of surface-mounted or submerged impermeable horizontal membrane wave barriers was tested with various membrane tensions, widths, and submergence depths. It was seen that an optimal combination of design parameters existed for given water depths and wave characteristics. From the present study, it can be concluded that a properly designed horizontal flexible membrane can be a very effective wave barrier and its optimal design can be found through a comprehensive parametric study using the developed theory and computer programs. To further verify its practicality, a more rigorous nonlinear time-domain numerical analysis and larger-scale experiments need to be done.

REFERENCES

Abul-Azm, A.G., 1994. Wave diffraction by double flexible breakwaters, *J. Applied Ocean Res.*, **16**, pp. 87-99.

Aoki, S., Liu, H. and Sawaragi, T., 1994. Wave transformation and wave forces on submerged vertical membrane *Proc. Intl. Symp. Waves-Physical and Numerical Modeling*, Vancouver, pp. 1287-1296.

Cho, I.H. and Hong, S.W., 1995. Scattering of oblique waves by an infinite flexible membrane breakwater, *J. Korean Soc. of Coastal and Ocean Engrs.*, **7**(3), pp. 219-226 (in Korean).

Dean, R.G. and Dalrymple, R.A., 1991. *Water wave mechanics for engineers and scientists,* World Scientific.

Dalrymple, R.A., Losada, M.A. and Martin, P.A., 1984. Reflection and transmission from porous structures under oblique wave attack, *J. Fluid Mech.*, **224**, pp. 625-644.

Hagan, C.L., 1994. A theoretical/experimental study of a perforated wall wave absorber, *M.S. Thesis*, Texas A & M University, College Station.

Isaacson, M., 1991. Measurement of regular wave, *J. Waterway, Port, Coastal and Ocean Engrg.*, **117**(6), pp. 553-569.

Kee, S.T. and Kim, M.H., 1997. Flexible membrane wave barrier. Part 2. Floating/submerged buoy-membrane system, *J. Waterway, Port, Coastal and Ocean Engrg.*, **123**(2), pp. 82-90.

Kim, M.H. and Kee, S.T., 1996. Flexible membrane wave barrier. Part 1. Analytic and numerical solutions, *J. Waterway, Port, Coastal and Ocean Engrg.*, **122**(1), pp. 46-53.

Kim, M.H., Edge, B.L., Kee, S.T. and Zhang, L., 1996. Performance evaluation of buoy-membrane wave barriers, *Proc. 25th. Coastal Engrg. Conf.*, ASCE, Orlando, Florida.

Lee, J.F. and Chen, C.J., 1990. Wave interaction with hinged flexible breakwater, *J. Hydraulic Res.*, **28**, pp. 283-295.

McIver, M., 1985. Diffraction of water waves by a moored, horizontal, flat plate, *J. Engrg. Mathematics*, **19**(4), pp. 297-320.

Newman, J.N., 1994. Wave effects on deformable bodies, *J. Applied Ocean Res.*, **16**, pp. 47-59.

Siew, P.F. and Hurley, D.G., 1977. Long surface waves incident on a submerged horizontal plate, *J. Fluid Mech.*, **83**, pp. 141-151.

Thompson, G.O., Sollitt, C.K., McDougal, W.G. and Bender W.R., 1992. Flexible membrane wave barrier, *Proc. Conf. Ocean V*, ASCE, College Station, pp. 129-148.

Williams, A.N., Geiger, P.T. and McDougal, W.G., 1991. Flexible floating breakwater, *J. Waterway, Port, Coastal and Ocean Engrg.*, **117**(5), pp. 429-450.

Williams, A.N., 1996. Floating membrane breakwater, *J. Offshore Mechanics and Arctic Engrg.*, **118**, pp. 46-51.